New Approach on Quantification of Porosity of Thin Films via Electron-Excited X-ray Spectra

New Approach on Quantification of Porosity of Thin Films *via* Electron-Excited X-ray Spectra

Erik Ortel,[*,†] Andreas Hertwig,[†] Dirk Berger,[‡] Pasquale Esposito,[§] Andrea M. Rossi,[§] Ralph Kraehnert[‡] and Vasile-Dan Hodoroaba[†,*]

[†]Federal Institute for Materials Research and Testing (BAM), Berlin 12200, Germany
[‡]Technische Universität Berlin, Straße des 17. Juni 135, 10623 Berlin, Germany
[§]Istituto Nazionale di Ricerca Metrologica, Strada delle Cacce 91, 10135 Turin, Italy
* erik.ortel@bam.de; dan.hodoroaba@bam.de

ABSTRACT

One of the crucial characteristics of functionalized thin films is their porosity, i.e. the ratio between the pore volume and the volume of the whole film. Due to the very low amount of material per coated area corresponding to thin films, it is a challenge for analytics to measure the film porosity. In this work we present an approach to determine the porosity of thin films by means of electron probe microanalysis (EPMA) either by wavelength dispersive X-ray spectrometry (WDX) or by energy dispersive X-ray spectrometry (EDX) at a scanning electron microscope (SEM). The procedure is based on the calculation of the film mass deposition from electron excited X-ray spectra. The mass deposition is converted into film density by division of measured film thickness. Finally, the film porosity is calculated from the measured film density and the density of bulk, non-porous film material. The general applicability of the procedure to determine the porosity is demonstrated on thin templated mesoporous TiO_2 films, dip-coated on silicon wafer, with controlled porosity in the range of 15 to 50%. The high accuracy of the mass deposition as determined from X-ray spectra was validated with independent methods (ICP-OES and weighing). Furthermore, for the validation of the porosity results, ellipsometry, interference fringes method (IFM) and focused ion beam (FIB) cross-sectioning were employed as independent techniques. Hence, the approach proposed in the present study is proven to be suited as a new analytical tool for non-destructive, accurate and relatively fast determination of the porosity of thin films.

Keywords: porosity, X-rays, EDX, thin film, TiO_2, density, mass deposition, STRATAGem

INTRODUCTION

Porosity is undoubtedly one of the factors that influences the physical interactions and chemical reactivity of solids with gases and liquids for many industrial, large-scale applications like catalytic coatings[1-3], electrocatalysis[4-5], solar cells[6], biomedical devices[7], supercapacitors[8-9] and sensors[10]. The porosity (*P*) can be defined as the fraction of pore volume (V_{pore}) relative to the total volume (V_{total}) or, alternatively, in terms of density, as one minus the ratio between total density (ρ_{total}) of the material and the bulk density of the pore wall (ρ_{bulk}):

$$P = \frac{V_{pore}}{V_{total}} = 1 - \frac{\rho_{total}}{\rho_{bulk}} \quad (1)$$

The determination of the porosity of solid materials can be performed, traditionally, by pycnometry and gas adsorption methods. The results are mostly accurate; however, the quantity measured is the so-called open porosity, quantifying only the volume of those pores which are accessible to liquid or gas. The accurate assessment of the overall porosity, including the fraction of closed pores, can be carried out usually only after grinding the material. Furthermore, in cases of thin films, these conventional methods fail due to the very small amount of material per coated area - defined as

mass deposition expressed in µg/cm^2. It should be noted that similar terms to "mass deposition" are "mass coverage", "mass coating" or "mass thickness" (all expressed in µg/cm^2).

Up to now, only few analytic techniques are available for porosity determination of thin porous films.[11] Methods used on a routine basis are gas sorption[12], electron microscopy[13] and ellipsometry[14-16]. Other techniques such as Rutherford backscattering spectrometry[13], X-rays methods (X-ray reflectometry, X-ray absorption and X-ray fluorescence)[16-19] and neutron reflectometry[20-21] have been also reported. Each analytical method is associated with benefits and drawbacks resulting from the specifics of the physical principle underlying the porosity measurement. For example, gas adsorption experiments, often based on measuring Nitrogen isotherms at 77 K, need a minimum sample amount with a total pore volume of about 1 cm³ to 10 cm³, which often cannot be reached for thin films. Electron microscopy allows the analysis of the porosity via direct observation of the pore geometry of two-dimensional (2-D) projections of thin film cross-sections[13], or by electron tomography of a representative volume of the film material.[22] Both techniques require elaborate sample preparation which may also change the initial pore morphology. Moreover, a special attention has to be paid to the appropriate setting of the threshold at the boundary between pore and pore wall in the electron micrographs.[18]

In spectroscopic ellipsometry, a technique used for validation purposes in the present study, the change in polarisation of the incident radiation is exploited to extract film properties by comparing with a model. The porosity is defined as the mixing ratio between material and air.[23-24] The mixing ratios of different media can be determined by using the Effective Medium Approximation (EMA) method.[25] A further optical method employed here, called interference fringes method (IFM), takes advantage from direct illumination of sufficiently thin porous samples, which causes multiple reflections of light at the layer(s) interfaces. This phenomenon results into constructive and destructive interference effects, which lead to the formation of a regular interferometric optical pattern (Fabry-Pérot fringes)[26]. Once an interference spectrum is obtained, all the optical constants of the film can be calculated – similarly to ellipsometry - by the EMA theory as the Bruggeman's model, which has been shown to predict porosity of porous films with known thickness, in good agreement with gravimetric determination[27]. To determine the film porosity by the two optical methods, the layer must be flat, reflective and transparent; moreover, the pores must be much smaller than the light wavelength, otherwise, incoherent light scattering will dominate the spectrum.

In the present paper we present a new alternative approach to determine the film porosity by electron probe microanalysis (EPMA), either to be employed by means of wavelength dispersive X-ray spectrometry (WDX) or energy dispersive X-ray spectrometry (EDX) at a scanning electron microscope (X-ray@SEM). The general approach is based on the calculation of the mass deposition of thin coatings determined from X-ray spectra containing X-ray lines of film and substrate. The mass deposition is converted into film density by division of measured film thickness. Finally, the film porosity is calculated from the measured porous film density and the density of bulk, non-porous film material. Compared to sorption experiments, there is no distinction between open and closed pores, because the X-ray spectra are emitted by the atoms in the entire film, independent of their location. From the X-ray spectra the total number of emitting atoms in the film can be calculated, and hence, the mass deposition of the porous film can be finally extracted. To our knowledge, the determination of the film porosity by means of electron excited X-ray spectrometry (WDX or EDX) has been nowhere reported yet.

The general procedure to determine the porosity is demonstrated on thin mesoporous TiO_2 model films, dip-coated on silicon wafer, following a template synthesis approach which allows controlling of both the pore size [28-29] and the porosity [29]. We first discuss the methodical approach, and then pre-characterize the porous TiO_2 model films. Afterwards, the determination of the mass deposition of a film with high porosity as training sample is discussed. In the last part of the paper we discuss the porosity results obtained after testing our approach on templated films with systematically adjusted porosity and validation by independent methods.

METHODICAL APPROACH

The new methodical approach for the determination of the film porosity is illustrated in Figure 1. The overall approach involves: The determination of the film mass deposition by X-ray@SEM analysis, and the determination of the film thickness by e.g. cross section imaging in SEM. From the mass deposition and the coating thickness, the average density of the film is calculated. This information, combined with the results for bulk, non-porous films is used to calculate the film porosity according to equation (1). In this study, the obtained mass deposition is validated by independent measurements by weighing and ICP-OES and the porosity results were counterchecked by the independent methods ellipsometry, IFM and SEM on FIB-prepared cross-section film images.

The mass deposition of thin films can be determined from X-ray spectra by using dedicated thin film analysis programs or using Monte-Carlo simulations[30]. In our study, we applied a quantification model originated from the work of Pouchou and Pichoir,[31] implemented in the thin film analysis software package STRATAGem[31]. The program iteratively fits calculated *k*-values of X-ray lines to measured ones whereas mass deposition and elemental composition are set as unknown parameters. The so-called *k*-values are the ratio of the X-ray line intensity of an element in the unknown sample to the X-ray line intensity of the same element in a sample (standard) with known elemental concentration. To obtain a good fit of the measured *k-values*, typically, three to four different accelerating voltages are sufficient. Note that all the elements in layer and substrate must be known *a-priori*, i.e. identified in the X-ray spectra. The accelerating voltages must be chosen in such a way that both the X-rays of the film elements and those of the substrate elements have acceptable signal-to-noise ratios. This depends on the material combination and layer thickness involved. The electrons used for the analysis must possess enough energy to penetrate the entire film into the underlying substrate so that enough X-rays are generated in the substrate. Conventionally, the thin film analysis software converts the mass deposition into film thickness after specification of film density. We use the inverse way and convert the mass deposition into film density by measuring the film thickness.

The good reliability of elemental composition as determined by X-ray@SEM analysis using the Pouchou and Pichoir model has been proven for various layered materials such as Ni-Si films on Si[32], Fe-Ni alloy thin films on Si[33-34], sulfur segregation in Ni and Ni alloys[35], Pd-Ni-Co alloy films on Si[36], Pt and Ni films on Si[37] and Carbon layer on Si, Al and brass[38]. Hodroj et al.[39] found good agreement of measured film densities by X-ray@SEM of non-porous TiO_2-SiO_2 films to independently determined film densities by X-ray reflectometry and ellipsometry. The interlaboratory comparison in [33-34] on test and reference Fe-Ni thin film systems could demonstrate that the elemental fractions in the layer as determined by STRATAGem have associated measurement uncertainty in the range of about 4 rel.-% (at a confidence level of 95%).

EXPERIMENTAL

Chemicals.

$TiCl_4$ (99.9 %) was obtained from Acros and ethanol was purchased from Roth. The polymer template poly(ethylene oxide)$_{100}$-*b*-poly(propylene oxide)$_{70}$-*b*-poly(ethylene oxide)$_{100}$ (Pluronic F127, labeld as PEO-PPO-PEO) was purchased from Sigma-Aldrich. The polymer template poly(ethylene oxide)$_{213}$-*b*-poly(butadiene)$_{184}$-*b*-poly(ethylene oxide)$_{213}$ (labelled as PEO-PB-PEO) is from Polymer Service Merseburg GmbH. All chemicals were used without further purification. Si wafers were employed as substrates for film deposition. Before dip-coating, Si wafers were cleaned with ethanol. Polished bulk, pure Ti (Micro-Analysis Consultants LTD., registered standard No. 1479) and a Si-wafer (undoped (111) University Wafer) served as reference materials (standards) for EDX measurements to determine the *k-values* corresponding to the elements present in the layer and substrate.

Synthesis of model films.

TiO_2 films were synthesised following a synthesis strategy called Evaporation Induced Self Assembly (EISA)[40], which based on polymer templates and a TiO_2 precursor. This synthesis strategy allows controlling of both the pore size by the applied polymer molecular mass[28-29] and the porosity by

adjusting the template-to-precursor ratio in the synthesis[29]. TiO_2 films with five different porosities were synthesized as illustrated in Figure 2:

a) one training film templated with PEO-PPO-PEO, resulting in a film with small mesopores and high porosity

b) three test films templated with PEO-PB-PEO, with larger mesopores and varied amount of template resulting in films with controlled porosities

c) one untemplated TiO_2 reference film, synthesised identically to the templated films, which serves as a compact, non-porous reference material designed to determine the bulk TiO_2 film density.

Dip coating solutions were prepared by first adding $TiCl_4$ (1.0 g) to stirred dry ethanol (5 mL). In a second solution the polymer template was dissolved in a mixture of ethanol (5 mL) and water (0.8 mL). Then both solutions were joined. The template mass in the dip coating solutions was adjusted to 38, 188, 375 mg for the PEO-PB-PEO templates. When PEO-PPO-PEO was employed as a template, 750 mg was used. To synthesize a compact, non-porous untemplated TiO_2 film no template polymer was added to the solution. Dip coating was performed in a controlled atmosphere at 25 °C and 40 % relative humidity (r.h.) for the PEO-PPO-PEO templated film and 25 °C and 20 % r.h. for the PEO-PB-PEO and the untemplated films. All films were drawn out from the dip-coating solution with a withdrawal rate of 60 mm/min. Thereafter, samples were conditioned at 80 °C for 4 h in a tube furnace. To finally remove the templates and crystallize the TiO_2 pore wall, the temperature was raised at 1 °C min^{-1} to 475 °C.

Pre-characterization of model films and measurement of film thickness.

In order to demonstrate that the applied synthesis procedure yields TiO_2 films with homogenous controlled porosity, the layers were characterized by SEM, SAXS (small-angle X-ray scattering) and TEM. The pore morphology and film thickness were analyzed with a SEM Carl Zeiss Supra 40 equipped with a Schottky field emitter. The film thicknesses were measured by imaging of fractured film of the coated Si wafers. Two-dimensional SAXS patterns were recorded on a Bruker Nanostar instrument with a three-pinhole collimation system, using a copper anode as X-ray source (Cu Kα radiation), a 2D detector (2-D HI STAR of 1024x1024 pixels) with a sample-to-detector distance of 670 mm and employing a sample holder that enabled rotation of the sample between 90° and 5° relative to the incident beam. For SAXS measurements a respective PEO-PPO-PEO templated TiO_2 film was coated on 50 µm thin silicon wafers. Crystallinity of film fragments removed from the Si substrate was studied by TEM on an FEI Tecnai G2 20 S-TWIN instrument operated at 200 kV.

Porosity analysis by X-ray@SEM.

Measurement of X-ray spectra.

The measurements of the X-ray spectra were performed with an energy dispersive X-ray spectrometer (EDS) with a 100 mm^2 silicon drift detector (SDD) of type UltraDry from Thermo Scientific™. For the calculation of *k-values* ($I_{unknown}/I_{standard}$) all net peak X-ray intensities of interest were divided by live time (600 s) and electron probe current. All spectra were measured under the same geometrical conditions. The *k-values* of Ti Kα and Si Kα corresponding to the TiO_2 films were determined at following accelerating voltages: 7, 10, 15, 20 and 30 kV.

Evaluation of mass deposition.

The mass deposition were calculated by STRATAGem film analysis software (version 2.6, SAMx, Guyancourt, France) by manual data input of the measured *k-values*. The fraction of Oxygen was set as corresponding to the atomic stoichiometry ratio of TiO_2.

Calculation of film density and porosity.

Based on the determined mass deposition and the measured film thickness, the density was calculated according to the formula in Figure 1 (“density box”). To calculate the film porosity, the density of the untemplated non-porous film material was evaluated as bulk density. Finally, the film

porosity was calculated by dividing the two film densities, of the porous, templated film by that of the non-porous, compact, untemplated film according to the formula in Figure 1 ("POROSITY box").

Validation of mass deposition by ICP-OES and weighing.

The mass deposition of PEO-PPO-PEO templated TiO_2 film coated on a 3 x 3 cm^2 silicon wafer was determined by analyzing the Ti concentration of the dissolved layer in a 715-ES-inductively coupled plasma (ICP-OES) system (Varian). The TiO_2 film were dissolved by acid hydrolysis in a 1:1 mixture of H_2SO_4 (95 wt.-%) and H_3PO_4 (85 wt %) at 200 °C and 20 bar in a microwave chamber at 200 W for 30 min. The mass deposition was further determined by weighing the PEO-PPO-PEO templated TiO_2 film by a micro-balance of type Sartorius 4503. The same substrate was weighed before and after dissolving the TiO_2 film by acid hydrolysis.

Validation of porosity results by ellipsometry, IFM, FIB cross-section.

Ellipsometry.

All spectroscopic ellipsometry measurements on the samples in this study were carried out with a M2000DI goniospectral ellipsometer (J. A. Woollam Co.). The instrument has a spectral range from 192 nm to 1692 nm with 710 distinct wavelengths and a circular measured area of roughly 3 mm diameter. All samples were measured with an angle of incidence from 50° to 75° in steps of 5°. The data analysis and fitting process was performed with the WVASE32 software (ver. 3.810). For the data analysis the Bruggeman model[41] was used as it is the model usually implemented in ellipsometry analysis code that is applicable over a large range of mixing ratios between two phases in order to calculate the porosity.[42] The mixed phase investigated here consists of TiO_2 and air (void). This means a very large refractive index contrast and, hence, a significant influence of scattering on the measurement result. Estimating a nominal mean size of the voids in the range of 10 nm in the TiO_2 matrix, it was decided to use only the long wavelength part of the spectrum in the range between 300 nm and 1000 nm. This restriction of the wavelength range applied to all samples. The dielectric functions of Si was taken from [43]. The dielectric function of the TiO_2 material was developed as a multi-peak oscillator model using four Gaussian absorption bands throughout the UV part of the analysed wavelength range. The absorption coefficient *k* was essentially 0 above 400 nm - as expected for clean TiO_2. The multi-sample analysis assumes that the dielectric function of the TiO_2 matrix does not change over the samples, i.e. the only varying parameter between the different layers is the EMA mixing ratio. Thus, the same model for the dielectric function of the matrix was used for all samples and this part of the overall model could be optimised using the very large dataset obtained on all samples. Due to the complexity of this analysis, a systematic evaluation of measurement uncertainty (e. g. by means of a sensitivity analysis or a Monte-Carlo simulation) is impossible. The uncertainties given in this work are the result of a best-of-knowledge estimate taking into account the figure of merit (mean square error, MSE) value of the fit for the different samples. After strict model simplification, the total number of fit parameters in the combined analysis was 29.

IFM.

The samples were mounted into a Leica inverted microscope and illuminated with focused (4x, 0.1 NA) white light by a mercury discharge lamp. Reflected light was collected through the same lens positioned along an axis normal to the surface and then transmitted to a CCD-based spectrometer. Reflectance spectra were collected in a circular spot (diameter ~1 mm) at the center of the samples. All the samples show characteristic and repeatable interference patterns for which software (SCOUT) simulation of the optical constants was attempted.

FIB cross-section.

For the direct observation of the porosity in an SEM, cross sections of the test layers were prepared using a focused ion beam (FIB FEI Helios NanoLab 600). Conventional recipes for the cross section preparation are not successful since the porosity is affected by the energy impact of the ion beam. Standard ion beam energies between 16 and 30 keV are not useful even at the smallest beam

currents of several pA. At these energies the pore walls are melted and most of the pores at the surface of the cross section disappear. Only at an ion beam energy of 5 keV and a beam current well below 50 pA the pores are not destroyed. To prevent the damage of the porous layer, 1 µm protection layer of platinum is deposited by electron beam induced metalorganic vapor phase epitaxy (MOCVD). The porosity is then imaged using ultra-high resolution SEM at 1 keV or below and a very small working distance. To determine the porosity from 2D projection from film cross sections prepared by FIB, the micrographs were image processed by the software package ImageJ[44]. Specifically, to remove the variation in brightness and the noise, the images were processed with a FFT bandpass filter (large structures down to 40 pixels and small structures up to 10 pixels). The average "2D porosity" is measured from the filtered images by thresholding to a grayscale value that distinguishes features that correspond to a pore (assigned as 1 value) from the pore wall (assigned as 0 value). An example of the porosity determination by FIB cross-sectional images is shown in the supplementary information Figure S1. The 2D projection of the pore volume is identical to "3D porosity" only for isotropically distributed structures. Templated films synthesized by EISA show typically ordered pore geometry.[40] Therefore, FIB milling was performed on five randomly chosen film positions to extract statistically relevant information over different ordered pore plains.

RESULTS AND DISCUSSION

Structural features of the model TiO_2 films.

To demonstrate that the applied synthesis method yields TiO_2 films with homogenous, controlled porosity and film thickness, the main structural features of the porous TiO_2 coatings synthesized were analysed. Figure 3 presents SEM micrographs, SAXS patterns and TEM images of the training film. The SEM micrograph of the film surface in Figure 3a shows a homogeneous film which is dominated by uniformly sized mesopores of nearly spherical shape of ca. 10 nm diameter. The fractured film of the coating in Figure 3b indicates that the pores are distributed homogeneously throughout the entire film depth. The total film thickness amounts to 180 nm.

SAXS yielded information on pore ordering. 2D-SAXS patterns recorded in transmission are shown in the insets in Figures 3a (at normal incidence) and 3b (at 5° incidence to the substrate surface). The SAXS pattern in the inset of Figure 3a clearly shows two isotropic diffraction rings, confirming mesoscopic ordering parallel to the substrate surface with *d*-spacing of ca. 11 nm and 7.4 nm. The 2D-SAXS pattern in the inset of Figure 3b shows off-specular reflections at *d*-spacing of ca. 4.3 nm. Such 2D-SAXS patterns can, for instance, be interpreted as a body-centered cubic mesostructure of spherically distorted mesopores in (110) orientation relative to the substrate.[45] Furthermore, the ellipsoidal shape of the patterns indicates a pore shrinkage perpendicular to the substrate by about 60%, which is commonly reported in literature for mesoporous oxide films.[46] Further, the crystallinity of the titania film was investigated by SAED (Figure 3c) and HRTEM (Figure 3d). Both the discrete diffraction rings in the SAED image (Figure 3 c) and the visible lattice planes in the HRTEM image (Figure 3d) evidence that the pore walls are crystalline. The positions of the diffraction rings (Figure 3c), as well as the lattice fringes observed in HRTEM (Figure 3d) are consistent with anatase as a crystalline phase.

To demonstrate that the new approach is applicable also to coatings with a broad range of film porosities, and also to validate the porosity results, TiO_2 films with significantly different porosities were synthesized as a test set of films. According to the synthesis procedure described in[29], we synthesized PEO-PB-PEO templated titania films with a step-wise increased concentration of the PEO-PB-PEO template in the $TiCl_4$-based dip-coating solution from 4 to 38 mass-% (mass ratio of template to $TiCl_4$). Figure S2 displays SEM images of the film surface, of the fractured film and of the FIB cross-section of the test films. Already at the lowest template concentration (4 mass-%), mesopores of about 20 nm in diameter are visible on the film surface. With increasing template concentration the pore size of about 20 nm remains unchanged (Figure S2), while the distance between pores decreases and, consequently, the film porosity increases. The film thicknesses as determined on the area of fractured film amount to 101, 110 and 125 nm.

To determine the bulk TiO_2 film density for porosity calculation, an untemplated TiO_2 film were synthesized identically to the templated films, but in absence of the pore-forming block-copolymer template (reference film). SEM images of the untemplated TiO_2 film are shown in Figure S3. In contrast to the templated coatings, the untemplated film synthesized without template does not possess a templated mesopore structure and contains small cracks and micropores (<2 nm). The film thickness amounts to 45 nm.

In conclusion, the analytic results confirm that templated mesoporous anatase films with homogenous pore structure and with different porosities could be synthesized. Moreover, an untemplated TiO_2 film with a nearly non-porous, compact structure could be realised. These coatings were used in the present study as model films to prove the new approach.

Mass deposition analysis of the training film.

To analyze the mass deposition of the TiO_2 training film, pre-characterized in the previous section, the intensity of the Si Kα and Ti Kα X-ray lines at various accelerating voltages was measured by EDX and the corresponding *k-values* were calculated. Figure 4 shows the *k-values* of the Si Kα and Ti Kα X-ray lines in dependence on the applied accelerating voltage (Figure 4a) and the *k-values vs.* film mass deposition for the various accelerating voltages applied (Figure 4b). The experimental determined *k-values* decrease for Ti Kα line of the film and increase for the Si Kα line of the substrate with increasing accelerating voltage (see the symbols in Figure 4a). Based on these experimental *k-values*, theoretical *k-values* of Si Kα and Ti Kα are iteratively calculated by the film analyzes software, with elemental composition and mass deposition as free parameters (see the continuous curves in Figure 4b). The small deviations of the calculated *k-values* from all the measured points indicate the robustness and validity of the Pouchou and Pichoir model implemented in the film analyses software for this layered system. The good fit quality affecting finally the accuracy of the film mass deposition is similar to other layer-substrate systems evaluated in literature.[33, 36-38] The resulting mean mass deposition of the TiO_2 training film is 30.6 µg/cm².

To validate this result, the mass deposition was independently determined by two other methods, ICP-OES and weighing. In particular, the titania film was dissolved in a acid mixture of H_2SO_4 and H_3PO_4 without affecting the Si substrate, and the Ti concentration was determined by ICP-OES. The resulting mass deposition of TiO_2 was 30 µg/cm². Moreover, the Si wafer was weighted before and after dissolving of the TiO_2 film by using a microbalance, which results in 32 µg/cm² mass deposition. Both values deviate less than 5% from the value of 30.6 µg/cm² obtained *via* the- X-ray@SEM analysis. Hence, the conventional analytical methods confirmed the evaluated mass deposition value.

Porosity of the training film.

Based on the determined mass deposition of 30.6 µg/cm² and the measured film thickness of 180 nm (Figure 3b), the density of the PEO-PPO-PEO templated film amounts to 1.7 g/cm³ (according to the formula in Figure 1).

To calculate the film porosity, the density of bulk, non-porous film material must be known. Therefore, the mass deposition of the untemplated TiO_2 film was determined identically as the templated film and amounts to 15 µg/cm². By taking the film thickness of 45 nm (acc. to Figure S3b), the resulting untemplated film density is 3.4 g/cm³. The density of the crystalline phases of anatase is 3.84 g/cm³.[47] Hence, the determined density of the untemplated TiO_2 film, based on a $TiCl_4$/EtOH/H_2O-solution calcined at 475 °C, has a slightly lower value than commonly for anatase. That is expected for thin TiO_2 films, which show a higher degree of internal stress due to the sol-gel and calcinations synthesis steps[47], resulting also in small cracks and pores (see SEM top-view, Figure S3a).

Finally, the film porosity of the TiO_2 training film can be calculated by dividing the two film densities, of the porous, templated film by the non-porous, compact, untemplated one. Thus, (1-(1.7/3.4))*100% yields a porosity value of 49%. Grosso et al. determined a film porosity of 45% for a F127-$TiCl_4$-based TiO_2-film calcined at 400°C, and a porosity of 40% by ellipsometry and RBS,

respectively.[48] Hence, the determination of the porosity by the new X-ray@SEM approach shows good agreement to reported values of similar templated TiO_2 films in the literature. This concept demonstrates for the first time that the porosity of thin porous films can be quantitatively determined with high accuracy by a combined X-ray/SEM approach.

Test films with variable porosity for validation purposes.

To demonstrate that the new approach is applicable also to coatings with a broad range of film porosities, but also for purpose of validation of the results obtained, TiO_2 films with significantly different porosities were synthesized (see section **Structural features of the porous film**). The porosity results as determined by the X-ray@SEM approach were validated by the independent analytical techniques: ellipsometry, IFM and cross-section FIB analysis.

The measured film thickness by SEM of fractured film and the mass deposition by X-ray spectra, microbalance and ICP-OES as well as the corresponding film densities and porosities of all investigated films are summarized in Table 1. Also the type of template, template concentration and the resulting pore diameter are shown. The film thickness of the templated films increases from 45 to 175 nm (Table 1) with increasing concentration of the template in the dip-coating solution, i.e. with increasing viscosity. For the porosity values as determined by X-ray@SEM, ellipsometry, IFM and FIB cross-section corresponding measurement uncertainties have been roughly estimated. They vary over a range of maximum 10% and are mainly caused by measurement uncertainty associated to the film thickness (of max. +/- 5 nm) for the optical and X-ray methods or, respectively, by the uncertainty in setting the threshold for delimitation of the pores in the FIB cross-section micrographs. A graphical overview with all porosity data is offered in the diagram in Figure 5. The nearly monotone increase of the porosity of the test films, from 13% to 28% as measured by X-ray@SEM, with template concentration, is obvious. The training film is provided with a distinct, higher porosity of 49%. The same trend is revealed by the porosity values measured on the same films by ellipsometry, IFM and FIB cross-section images. If the porosity data obtained by all the applied techniques are compared, it can be concluded that the deviation between the film porosity values is smaller than 8%. This is a remarkable result, providing the validity of determination of the thin film porosity by the new X-ray@SEM approach.

CONCLUSION

The combined X-ray@SEM analysis with film thickness measurement is successfully proved as a new analytical tool for the non-destructive determination of the porosity of thin films. The approach relies on the determination of the mass deposition from electron excited X-ray spectra. The high accuracy results of calculated mass deposition are validated by measurements with independent methods (ICP-OES and weighing).

As demonstrated for thin mesoporous template TiO_2 films with variable porosity, the new approach shows good agreement with porosity values determined by other techniques (ellipsometry, IFM and FIB cross section) as well as with data of similar films as reported in the literature. The present analytical study constitutes a proof-of-concept for the challenging characterization of the porosity of thin films by means of electron excited X-rays. The approach may be applied for a wide range of coatings with variable pore structure and material composition. No special requirements such as knowledge of optical film properties are necessary. By knowing the number of layers, their succession and elements contained, i.e. identified in the spectra, also multilayer systems can be resolved quantitatively. Furthermore, the proposed X-ray@SEM method enables the assessment of µm-homogeneity of porosity over large film area. Automatic measurement of X-ray spectra at different positions is available at any modern SEM/EDX system; however, data evaluation is not yet automated.

Acknowledgment

This work was supported by the SETNanoMetro Seventh Framework Programme project (project number 604577; call identifier FP7-NMP-2013_LARGE-7). RK appreciates generous funding from BMBF under contract FKZ 03K3009 and Einstein Stiftung Berlin (EJF-2011-95).

References

1. Ortel, E.; Polte, J.; Bernsmeier, D.; Eckhardt, B.; Paul, B.; Bergmann, A.; Strasser, P.; Emmerling, F.; Kraehnert, R., *Applied Catalysis A: General* **2015**; *493*, 25-32.
2. Yang, Y.; Fei, H.; Ruan, G.; Tour, J. M., *Advanced Materials* **2015**; *27* 20, 3175-3180.
3. Ortel, E.; Sokolov, S.; Zielke, C.; Lauermann, I.; Selve, S.; Weh, K.; Paul, B.; Polte, J.; Kraehnert, R., *Chemistry of Materials* **2012**; *24* 20, 3828-3838.
4. Ortel, E.; Reier, T.; Strasser, P.; Kraehnert, R., *Chemistry of Materials* **2011**; *23* 13, 3201-3209.
5. Bernicke, M.; Ortel, E.; Reier, T.; Bergmann, A.; Ferreira de Araujo, J.; Strasser, P.; Kraehnert, R., *ChemSusChem* **2015**; *8* 11, 1908–1915.
6. Xiao, J.; Han, L.; Zhu, L.; Lv, S.; Shi, J.; Wei, H.; Xu, Y.; Dong, J.; Xu, X.; Xiao, Y.; Li, D.; Wang, S.; Luo, Y.; Li, X.; Meng, Q., *RSC Advances* **2014**; *4* 62, 32918-32923.
7. Kurtulus, O.; Daggumati, P.; Seker, E., *Nanoscale* **2014**; *6* 12, 7062-7071.
8. Yang, Y.; Li, L.; Ruan, G.; Fei, H.; Xiang, C.; Fan, X.; Tour, J. M., *ACS Nano* **2014**; *8* 9, 9622-9628.
9. Gu, L.; Wang, Y.; Lu, R.; Guan, L.; Peng, X.; Sha, J., *Journal of Materials Chemistry A* **2014**; *2* 20, 7161-7164.
10. Hotta, K.; Yamaguchi, A.; Teramae, N., *ACS Nano* **2012**; *6* 2, 1541-1547.
11. Sanchez, C.; Boissiere, C.; Grosso, D.; Laberty, C.; Nicole, L., *Chemistry of Materials* **2008**; *20* 3, 682-737.
12. Klotz, M.; Ayral, A.; Guizard, C.; Cot, L., *Journal of Materials Chemistry* **2000**; *10* 3, 663-669.
13. Liu, R.; Antoniou, A., *Acta Materialia* **2013**; *61* 7, 2390-2402.
14. Boissiere, C.; Grosso, D.; Lepoutre, S.; Nicole, L.; Bruneau, A. B.; Sanchez, C., *Langmuir* **2005**; *21* 26, 12362-12371.
15. Baklanov, M. R.; Mogilnikov, K. P.; Polovinkin, V. G.; Dultsev, F. N., *Journal of Vacuum Science & Technology B* **2000**; *18* 3, 1385-1391.
16. Soler-Illia, G. J. A. A.; Angelome, P. C.; Fuertes, M. C.; Grosso, D.; Boissiere, C., *Nanoscale* **2012**; *4* 8, 2549-2566.
17. Klotz, M.; Rouessac, V.; Rébiscoul, D.; Ayral, A.; van der Lee, A., *Thin Solid Films* **2006**; *495* 1–2, 214-218.
18. Clark, G. L.; Liu, C. H., *Analytical Chemistry* **1957**; *29* 10, 1539-1541.
19. Walker, C. T.; Mogensen, M., *Journal of Nuclear Materials* **1987**; *149* 2, 121-131.
20. Dourdain, S.; Bardeau, J.-F.; Colas, M.; Smarsly, B.; Mehdi, A.; Ocko, B. M.; Gibaud, A., *Applied Physics Letters* **2005**; *86* 11, 113108.
21. Wu, W.-l.; Wallace, W. E.; Lin, E. K.; Lynn, G. W.; Glinka, C. J.; Ryan, E. T.; Ho, H.-M., *Journal of Applied Physics* **2000**; *87* 3, 1193-1200.
22. Novak, V.; Ortel, E.; Winter, B.; Butz, B.; Paul, B.; Koci, P.; Marek, M.; Spiecker, E.; Kraehnert, R., *Chemical Engineering Journal* **2014**; *248*, 49-62.
23. Fried, M.; Lohner, T.; Polgar, O.; Petrik, P.; Vazsonyi, E.; Barsony, I.; Piel, J. P.; Stehle, J. L., *Thin Solid Films* **1996**; *276* 1-2, 223-227.
24. Albert, E.; Basa, P.; Deak, A.; Nemeth, A.; Osvath, Z.; Safran, G.; Zolnai, Z.; Horvoelgyi, Z.; Nagy, N., *Rsc Advances* **2015**; *5* 74, 60041-60053.
25. Tinga, W. R.; Voss, W. A. G.; Blossey, D. F., *Journal of Applied Physics* **1973**; *44* 9, 3897-3902.
26. Hernandez, G., *Fabry–Pérot Interferometers*. Cambridge University Press: Cambridge, **1986**.
27. Cai, W.; Shalaev, V., *Optical Metamaterials - Fundamentals and Applications*. Springer-Verlag New York: New York, **2010**.
28. Sokolov, S.; Ortel, E.; Kraehnert, R., *Materials Research Bulletin* **2009**; *44* 12, 2222-2227.

29. Ortel, E.; Fischer, A.; Chuenchom, L.; Polte, J.; Emmerling, F.; Smarsly, B.; Kraehnert, R., *Small* **2012**; *8* 2, 298-309.
30. Osada, Y., *X-Ray Spectrometry* **2005**; *34* 2, 92-95.
31. Pouchou, J.-L., *Microchim Acta* **2002**; *138* 3-4, 133-152.
32. Phung, T. M.; Jensen, J. M.; Johnson, D. C.; Donovan, J. J.; McBurnett, B. G., *X-Ray Spectrometry* **2008**; *37* 6, 608-614.
33. Hodoroaba, V.-D.; Kim, K. J.; Unger, W. E. S., *Surface and Interface Analysis* **2012**; *44* 11-12, 1459-1461.
34. Kim, K. J.; Unger, W. E. S.; Kim, J. W.; Moon, D. W.; Gross, T.; Hodoroaba, V. D.; Schmidt, D.; Wirth, T.; Jordaan, W.; van Staden, M.; Prins, S.; Zhang, L.; Fujimoto, T.; Song, X. P.; Wang, H., *Surface and Interface Analysis* **2012**; *44* 2, 192-199.
35. Christien, F.; Le Gall, R., *Surface Science* **2008**; *602* 14, 2463-2472.
36. Kühn, J.; Hodoroaba, V.-D.; Linke, S.; Moritz, W.; Unger, W. E. S., *Surface and Interface Analysis* **2012**; *44* 11-12, 1456-1458.
37. Procop, M.; Radtke, M.; Krumrey, M.; Hasche, K.; Schadlich, S.; Frank, W., *Anal. Bioanal. Chem.* **2002**; *374* 4, 631-634.
38. Galbert, F., *Microscopy and Microanalysis* **2007**; *13* SupplementS03, 96-97.
39. Hodroj, A.; Roussel, H.; Crisci, A.; Robaut, F.; Gottlieb, U.; Deschanvres, J. L., *Applied Surface Science* **2006**; *253* 1, 363-366.
40. Brinker, C. J.; Lu, Y. F.; Sellinger, A.; Fan, H. Y., *Advanced Materials* **1999**; *11* 7, 579-585.
41. Bruggeman, D. A. G., *Annalen Der Physik* **1935**; *24* 7, 636-664.
42. Fujiwara, H.; Koh, J.; Rovira, P. I.; Collins, R. W., *Physical Review B* **2000**; *61* 16, 10832-10844.
43. Herzinger, C. M.; Johs, B.; McGahan, W. A.; Woollam, J. A.; Paulson, W., *Journal of Applied Physics* **1998**; *83* 6, 3323-3336.
44. Schneider, C. A.; Rasband, W. S.; Eliceiri, K. W., *Nature Methods* **2012**; *9* 7, 671-675.
45. Ruland, W.; Smarsly, B. M., *Journal of Applied Crystallography* **2007**; *40*, 409-417.
46. Dutta, S.; Wu, K. C. W.; Kimura, T., *Chemistry of Materials* **2015**; *27* 20, 6918-6928.
47. Ottermann, C. R.; Bange, K., *Thin Solid Films* **1996**; *286* 1–2, 32-34.
48. Grosso, D.; Soler-Illia, G. J. d. A. A.; Crepaldi, E. L.; Cagnol, F.; Sinturel, C.; Bourgeois, A.; Brunet-Bruneau, A.; Amenitsch, H.; Albouy, P. A.; Sanchez, C., *Chemistry of Materials* **2003**; *15* 24, 4562-4570.

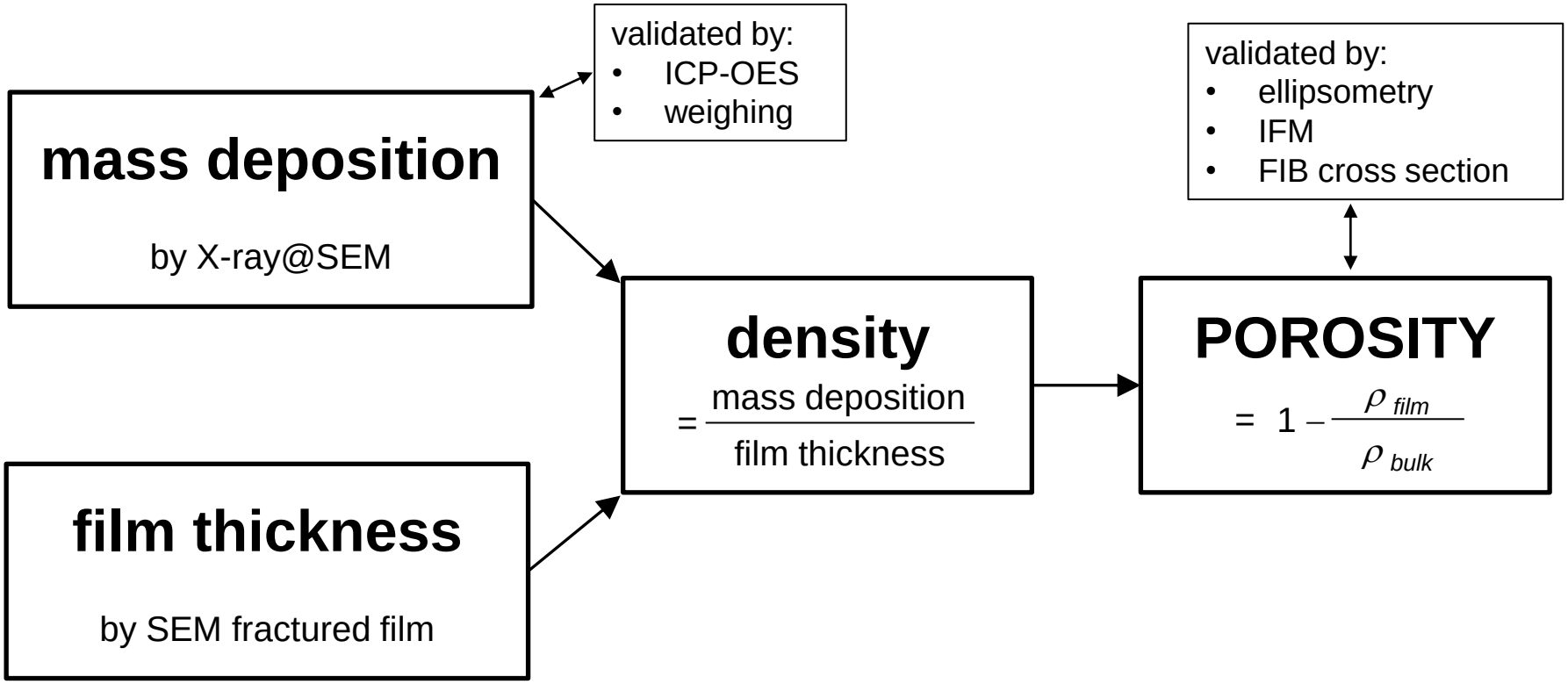

Figure 1: Approach to determine film porosity and the applied validation methods.

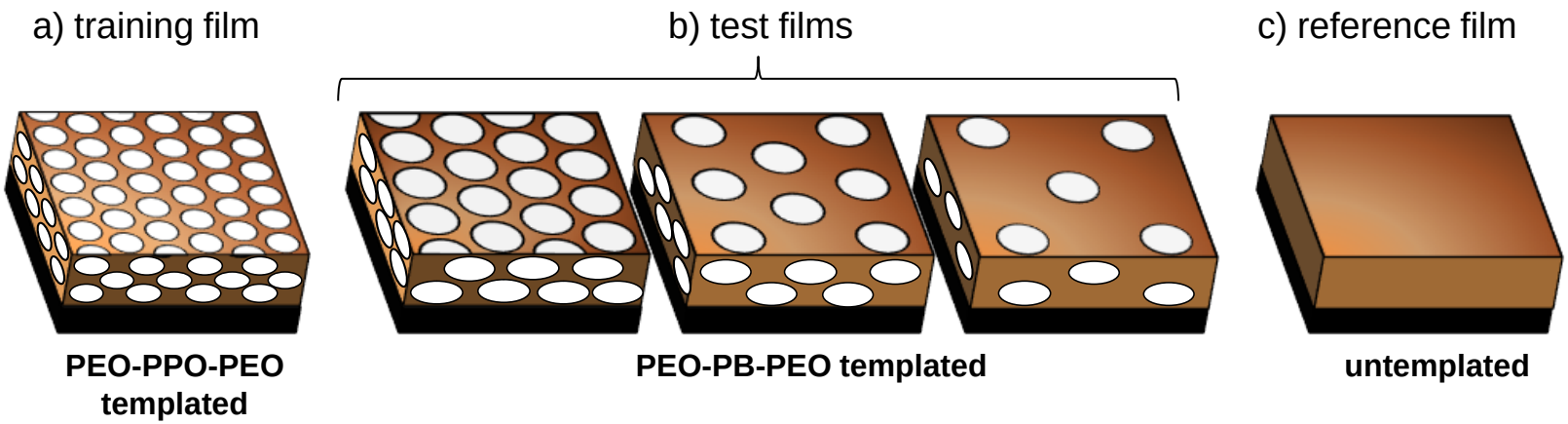

Figure 2:
TiO_2 films with five different porosities were synthesized, a) training film with small mesopores and high porosity, b) three test TiO_2 films with larger mesopores and varied porosities as well as c) an untemplated TiO_2 film, synthesized identically to the templated films, which serves as reference film for the TiO_2 film density.

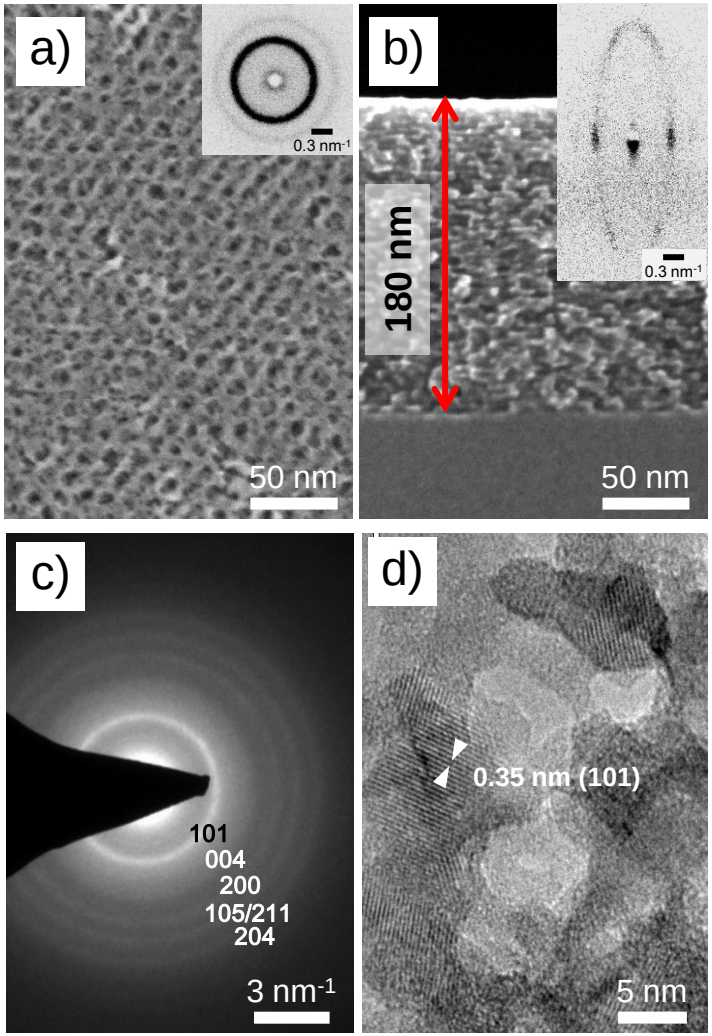

Figure 3: Investigation of the main structural features of the training TiO_2 film. a) SEM images of the film surface; b) SEM image of fractured film; c) SAED pattern and d) high resolution TEM analysis of film fragments. The insets in a) and b) show 2D-SAXS patterns recorded in transmission at a) normal and b) 5° incidence to the substrate surface.

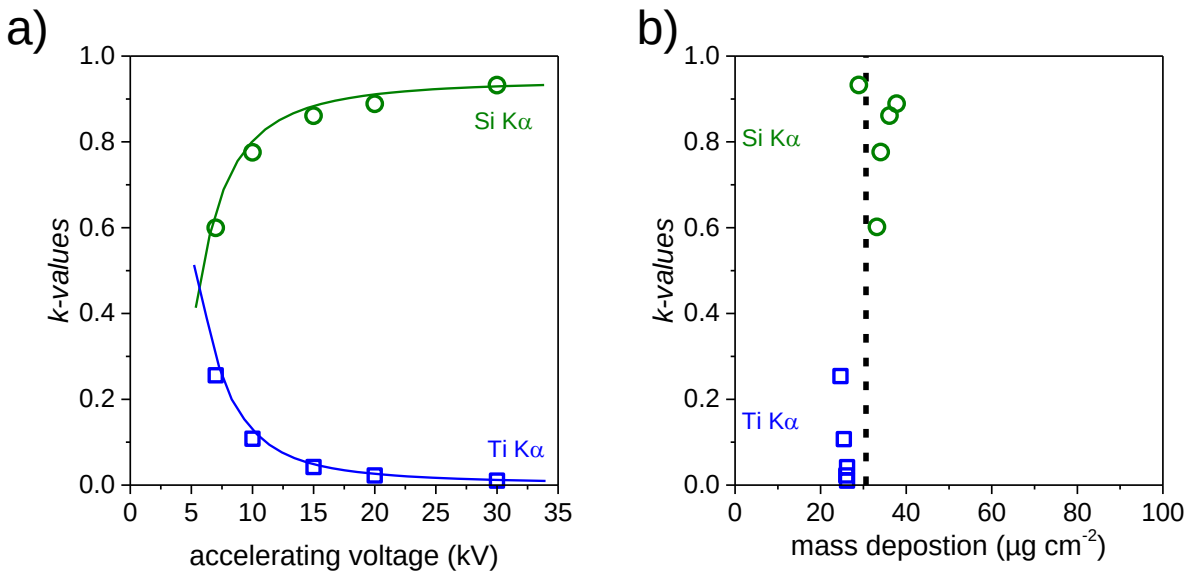

Figure 4: a) *k-values* of the Si Ka and Ti Ka vs. applied accelerating voltage, b) *k-values* versus calculated film mass deposition. Based on experimental *k-values*, theoretical k-values are iteratively calculated with elemental composition and mass deposition as free parameters (lines in a) so that the mean mass deposition of the TiO_2 training film can be finally extracted (see dashed line in b).

Table 1: Overview of all measured parameters of all investigated films: template concentration; used type of template; the measured pore diameter and film thickness by SEM; the mass deposition by X-ray@SEM, microbalance and ICP-OES; the film densities by X-ray@SEM and the porosities by X-ray@SEM, ellipsometry, IFM and FIB cross section.

template conc. (mass%)	polymer template	pore diameter (nm)	film thickness (nm)	mass depostion (µg/cm²)			film density (g/cm³)	porosity (%)			
		top view SEM	fracture area SEM	X-ray@ SEM	micro balance	ICP-OES	X-ray@ SEM	X-ray@SEM	ellipsometry	IFM	FIB cross section
75	PEO-PPO-PEO	10	180	30.6	32	30	1.7	49 ± 5	46 ± 7	n. m.	pores too small
38	PEO-PB-PEO	21	125	31.0	n. m.	n. m.	2.5	28 ± 5	32 ± 10	25 ± 7	28 ± 10
19	PEO-PB-PEO	23	110	29.3	n. m.	n. m.	2.7	22 ± 5	26 ± 7	19 ± 5	20 ± 10
4	PEO-PB-PEO	20	101	30.2	n. m.	n. m.	3.0	13 ± 5	14 ± 3	10 ± 3	12 ± 10
0	without	-	45	15.4	n. m.	n. m.	3.4	reference film			

n.m. = not measured

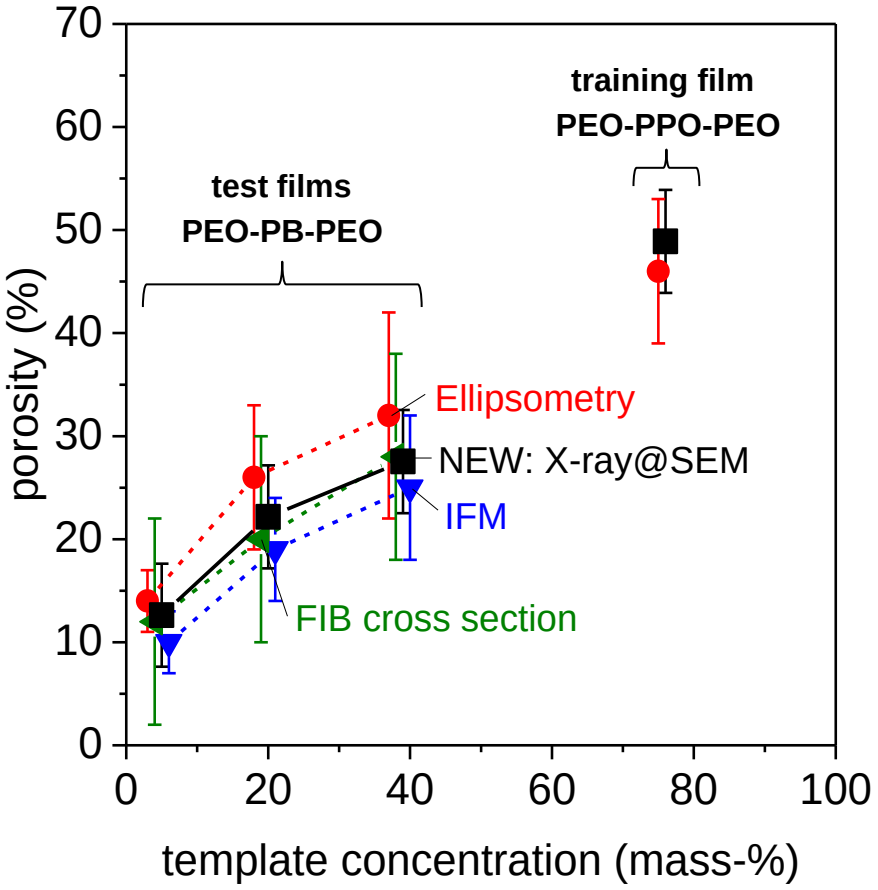

Figure 5: Porosity results determined by X-ray@SEM, ellipsometry, IFM and FIB cross section versus template concentration (mass-% template to $TiCl_4$) of polymer templated TiO_2 films.

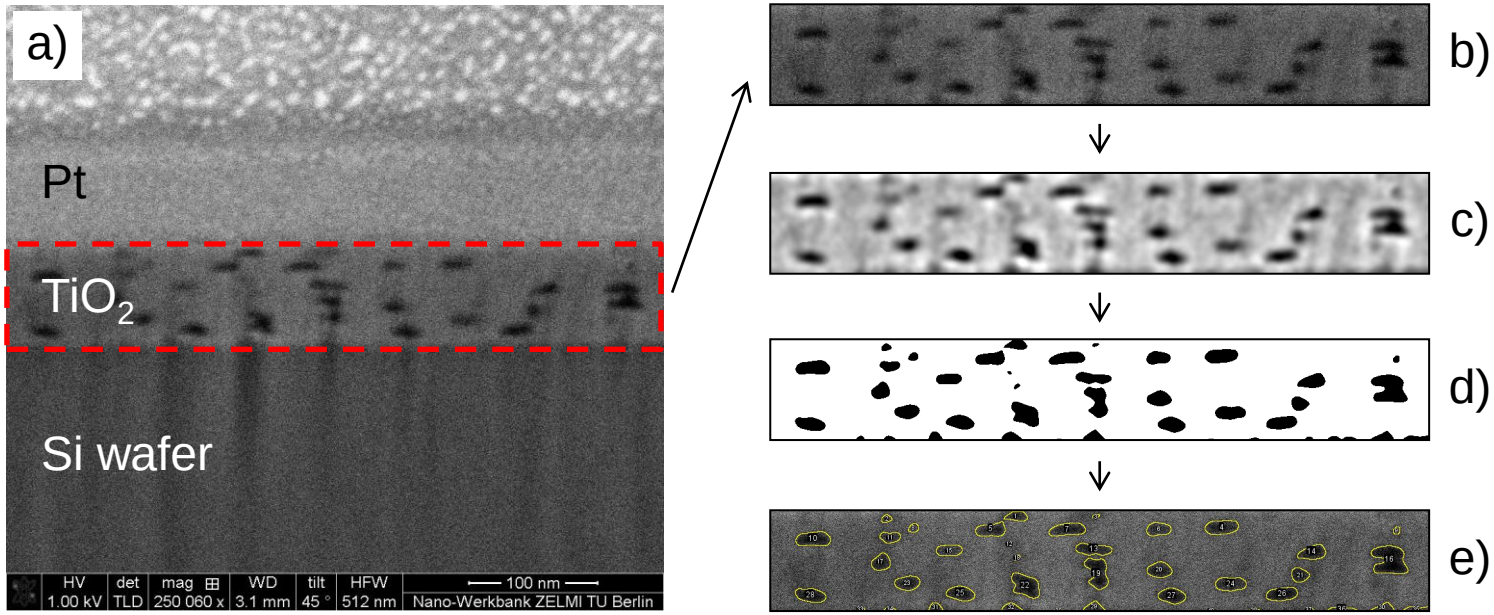

Figure S1: Data processing to determine the porosity of PEO-PB-PEO templated TiO_2 film (4 mass-% template) from a FIB-cross sectional prepared SEM image. a) original SEM image, b) selection of porous film area of interest, c) FFT bandpass filtered image (large structures down to 40 pixels and small structures up to 10 pixels), d) thresholding to a grayscale value that segregates the image to features that correspond to a pore (black) or a pore wall (white). e) Overlay of image b) with identified pores resulting in a porosity of 12%.

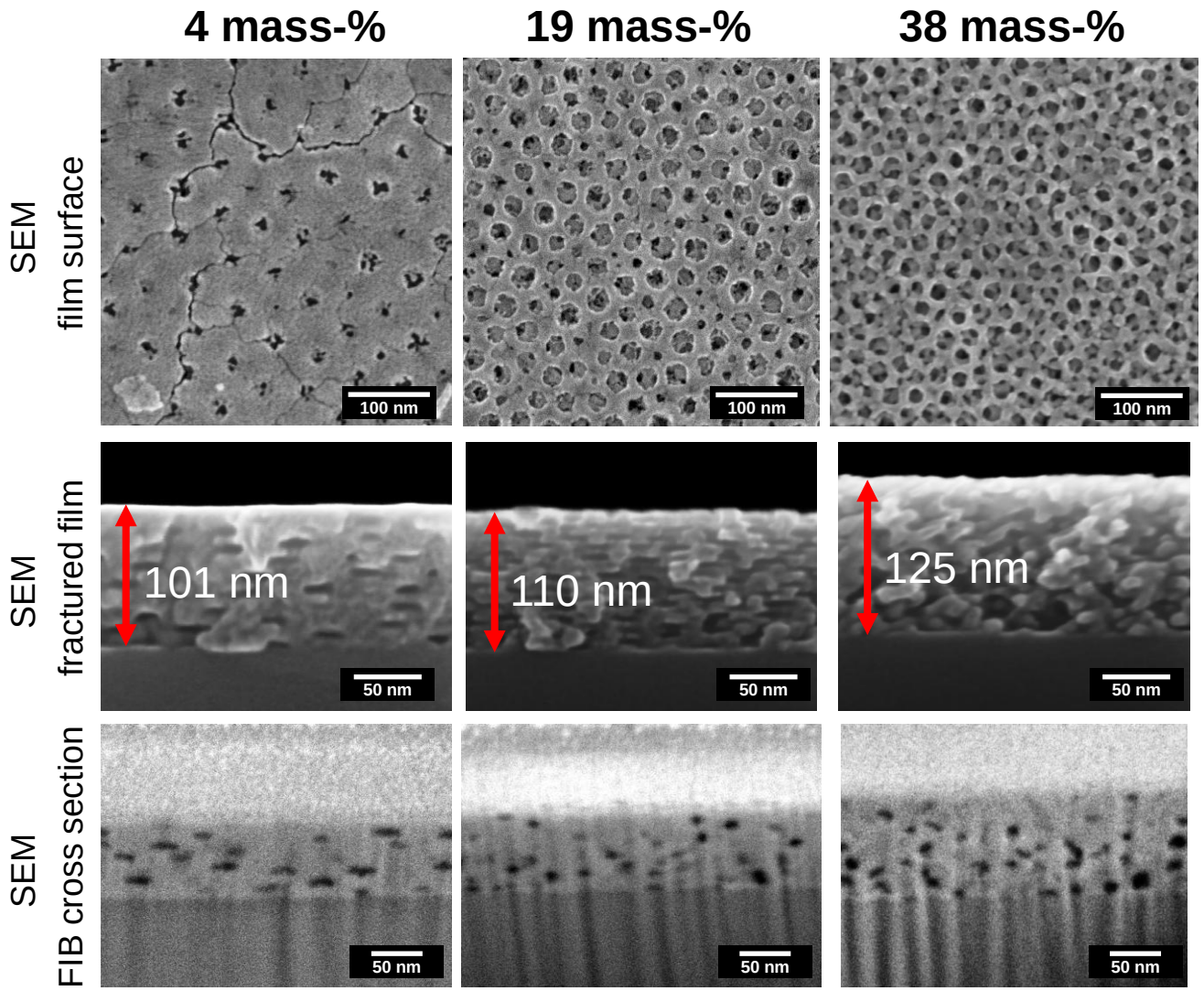

Figure S2: SEM images of the film surface (upper row), fractured film (middle row) and FIB cross section (lower row) of titania test films with increasing template concentration from left to right (4, 19, 38 mass-% PEO-PB-PEO to $TiCl_4$). With increasing template concentration the pore size of about 20 nm holds constant while the film porosity increases.

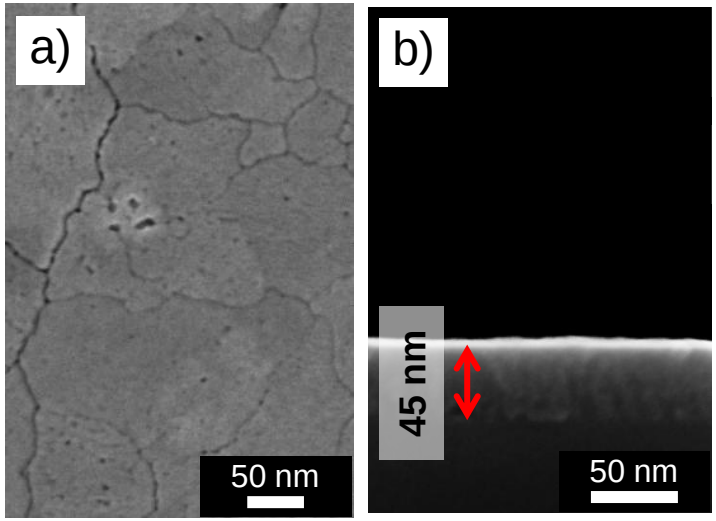

Figure S3: SEM images of untemplated TiO_2 film. a) top view and b) fractured film.

TOC

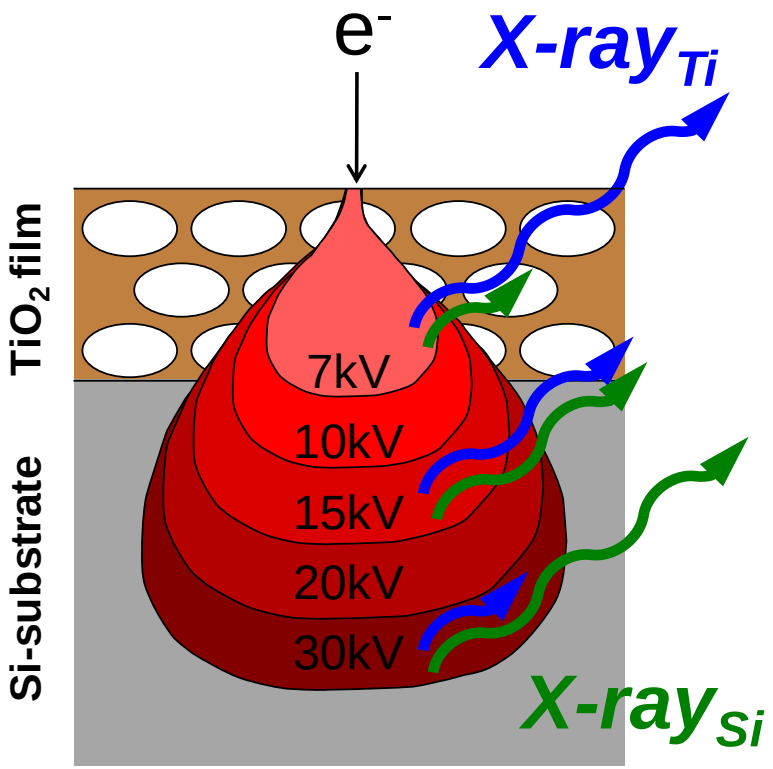
e-
X-ray Ti
TiO2 film
Si-substrate
7kV
10kV
15kV
20kV
30kV
X-ray Si